

Nonlinear Hall Effect in Insulators

Wen-Yu He^{1,*} and K. T. Law^{2,†}

¹*School of Physical Science and Technology, ShanghaiTech University, Shanghai 201210, China*

²*Department of Physics, Hong Kong University of Science and Technology, Clear Water Bay, Hong Kong, China*

(Dated: November 13, 2024)

The nonlinear Hall effect refers to the nonlinear voltage response that is transverse to the applied electric field. Recent studies have shown that the quantum geometric quantities on Fermi surfaces serve as fundamental contributors to the nonlinear Hall effect, suggesting that the nonlinear Hall effect occurs mainly in metals. However, in this work, we demonstrate that insulators can also exhibit the nonlinear Hall effect. We find that for an insulator driven at a finite frequency, a series of frequency dependent quantum geometric quantities from the occupied bands can give rise to a nonvanishing nonlinear Hall conductivity. The nonlinear Hall conductivity is frequency dependent: at resonance, it represents the inter-band transition enabled nonlinear Hall current; near resonance, it represents the nonlinear order polarization transverse to the electric field. We further connect the nonlinear Hall conductivity to the Kleinman conjecture in nonlinear optics and point out that the nonlinear Hall effect is generally allowed in insulators given the driving frequency near resonance. For the candidate materials, we consider the biased Bernal bilayer graphene under uniaxial strain and propose polarization resolved second harmonic microscopy to detect the nonlinear Hall effect there.

Introduction.— The Hall effect in materials is a fundamental phenomenon that not only has extensive practical applications [1–4] but also fosters a deeper understanding of topology, Berry curvature, and quantum geometry in electronic transport [3–7]. In recent years, the Hall effect has been extended beyond the linear regime to include the nonlinear response [8–26]. Importantly, it has been found that the nonlinear Hall effect in materials is closely related to the quantum geometric quantities on Fermi surfaces, including the Berry curvature dipoles [8], quantum metric dipoles [9–12] and their higher moments [16, 17]. Given its capability to probe the quantum geometry of Fermi surfaces [27–31], the nonlinear Hall effect is undergoing intensive investigations in a range of metals [27–43].

The nonlinear Hall effect that arises from the quantum geometry of Fermi surfaces is subjected to the constraint that the host material must have Fermi surfaces. The constraint stems from the intra-band consideration in the low frequency limit, which ignores the frequency dependent inter-band processes. It is conceivable that as the driving frequency increases to involve inter-band effects, the electronic states from the occupied bands can get excited or virtually excited to the unoccupied bands, which incorporates frequency dependent quantum geometric quantities in response to the driving electric field [44, 45]. Such inter-band processes bypass the constraint of Fermi surfaces, but their roles in the nonlinear Hall effect have yet been elucidated.

In this work, we show that in the frequency range involving inter-band processes, the driving electric field can induce the nonlinear Hall effect in a wide class of insulators. Specifically, as depicted in Fig. 1, we take the second harmonic generation (SHG) as a concrete example to illustrate how the nonlinear Hall effect occurs naturally in a *time reversal invariant insulator* as the driving

frequency approaches resonance. In the standard case of a time reversal invariant metal that exhibits the nonlinear Hall effect, the driving electric field at low frequency solely redistributes the electronic states near the Fermi surface (as seen in Fig. 1 (b)). The redistribution creates a net Berry curvature dipole [8] that generates the second harmonic Hall current in the metal. In the case that the metal is converted into an insulator with its valence bands fully occupied as depicted in Fig. 1 (c), a driving frequency exceeding the band gap enables an inter-band redistribution of the electronic states. During the inter-band processes, the electronic states from the fully occupied valence bands are excited onto the empty conduction bands and can generate the second harmonic Hall current. Importantly, even in the case that the driving frequency is slightly lower than the band gap (as seen in Fig. 1 (d)), the driving electric field can facilitate a virtual inter-band transition [44] and induce a second harmonic Hall polarization $\mathbf{P}_\perp(2\omega)$. By definition, the second harmonic Hall current has the form $\mathbf{J}_\perp(2\omega) = -2i\omega\mathbf{P}_\perp(2\omega)$, indicating that the second harmonic Hall polarization in an insulator is a clear manifestation of the nonlinear Hall effect. Notably, in the slightly off-resonant regime, the nonlinear Hall effect in an insulator is purely reactive and in principle has no optical absorption. Such nonlinear Hall effect in insulators without low energy dissipation is the key finding of this work.

In the following, we start from the density matrix formalism [46–49] to construct the second order nonlinear Hall conductivity and derive the explicit expression for the Hall component of the SHG. We show that in an insulator, a set of frequency dependent quantum geometric quantities are involved in the inter-band processes and contribute significantly to the second harmonic Hall conductivity as the driving frequency approaches resonance.

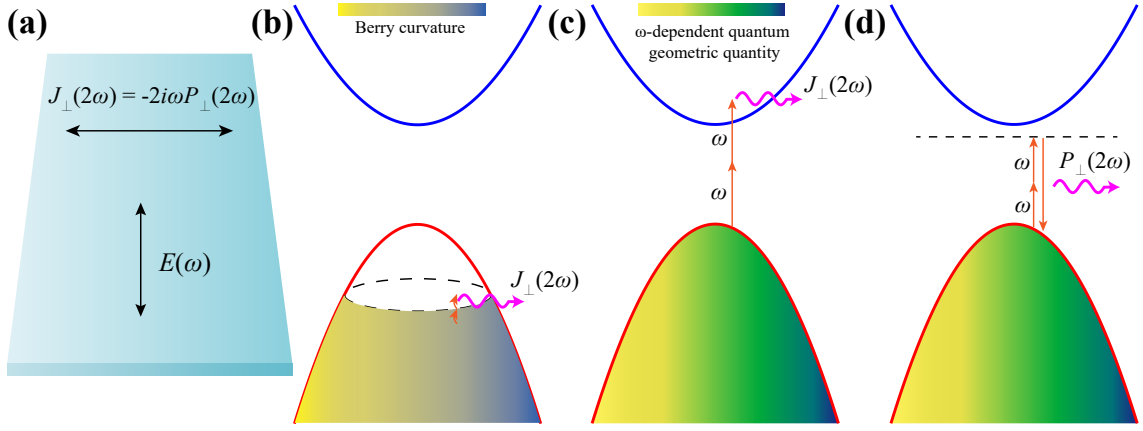


FIG. 1: Illustration of the nonlinear Hall effect in an insulator. (a) The SHG transverse to the applied electric field serves as a distinctive signature of the nonlinear Hall effect. (b) The Berry curvature dipole induced nonlinear Hall effect in a metal. The redistribution of electrons near the Fermi surface imbalances the Berry curvature and induces the nonlinear Hall effect. In (c) and (d), the valence bands get fully occupied and the system becomes an insulator. In the resonant regime in (c), electrons in the occupied bands are pumped onto the empty conduction bands, while in the slightly off-resonant regime in (d), electrons go through a virtual inter-band transition. In the inter-band processes, frequency dependent quantum geometric quantities in the occupied bands can give rise to finite $\mathbf{J}_\perp(2\omega)$ in (c) and finite $\mathbf{P}_\perp(2\omega)$ in (d) respectively. Both $\mathbf{J}_\perp(2\omega)$ and $\mathbf{P}_\perp(2\omega)$ manifest the nonlinear Hall effect.

Near resonance, the second harmonic Hall conductivity exhibits significant frequency dispersion, consistent with the Kleinman conjecture [50–52] in nonlinear optics that the overall permutation symmetry of the indices in the susceptibility breaks down due to the frequency dispersive properties of the material. The intrinsic connection between the Kleinman conjecture and the nonlinear Hall effect suggests that frequency-dispersive insulators are more likely to exhibit a pronounced nonlinear Hall effect. Finally, we calculate the nonlinear Hall conductivity in the bias gapped Bernal bilayer graphene under uniaxial strain and show that polarization resolved second harmonic microscopy can facilitate the detection of the nonlinear Hall effect in an insulator.

General theory for the nonlinear Hall effect.— To

study the second order nonlinear Hall effect, one needs to first extract the Hall component from the standard second order conductivity. In the second order response, it is well known that a linear polarized electric field $\mathbf{E}(t) = \mathcal{E}(\omega)e^{-i\omega t} + \mathcal{E}(-\omega)e^{i\omega t}$ can simultaneously induce both the SHG $J_q(2\omega) = \sigma_{qij}(2\omega; \omega, \omega)\mathcal{E}_i(\omega)\mathcal{E}_j(\omega)$ and the rectification $J_q(0) = \sigma_{qij}(0; \omega, -\omega)\mathcal{E}_i(\omega)\mathcal{E}_j(-\omega)$. Since the harmonic generation perpendicular to the applied electric field gives the most distinctive signature of the nonlinear Hall effect [27–41], in the below we will primarily focus on the Hall component of the SHG.

From the density matrix formalism [46–49], we know that the SHG conductivity in a two or three dimensional system ($d = 2, 3$) can be calculated as

$$\sigma_{qij}(2\omega; \omega, \omega) = \frac{e^3}{2\hbar} \int_{\mathbf{k}} \sum_a f_{a,\mathbf{k}} \left\{ \left[\hat{D}^i, \frac{1}{\hbar\bar{\omega} + \Delta E} \circ \left[\hat{D}^j, \frac{1}{2\hbar\bar{\omega} + \Delta E} \circ \left[\hat{D}^q, \hat{H}_0 \right] \right] \right] \right\}_{aa,\mathbf{k}} + (i \leftrightarrow j), \quad (1)$$

with \hat{D} being the covariant derivative operator [46, 49], \hat{H}_0 being the Hamiltonian, $\int_{\mathbf{k}} \equiv \int d\mathbf{k}/(2\pi)^d$, and $f_{a,\mathbf{k}}$ denoting the occupation of the Bloch state $|\psi_{a,\mathbf{k}}\rangle$. Here [...] means the commutator and $(\hat{A} \circ \hat{B})_{ab} = \hat{A}_{ab}\hat{B}_{ab}$ is the Hadamard product. We have assumed that the applied electric field is adiabatically switched on [46] so a phenomenological relaxation time is associated with the frequency: $\bar{\omega} = \omega + i\tau^{-1}$. As we focus on the SHG of an

insulator, the calculations are performed in the relaxation free limit: $\tau^{-1} \rightarrow 0^+$.

For $\sigma_{qij}(2\omega; \omega, \omega)$ in Eq. 1, it is evident that the two indices i and j are commutative, as is required by the intrinsic permutation symmetry [51, 52]. In contrast, the output index q is generally non-commutative with i and j . By definition, we know that the Hall conductivity corresponds to the anti-symmetric part when exchanging q with i and j . Thus, the Hall component of $\sigma_{qij}(2\omega; \omega, \omega)$

TABLE I: The explicit expressions of the second harmonic Hall conductivity. The Hall conductivity of the SHG takes the form $\sigma_{qij}^\perp(2\omega; \omega, \omega) = \epsilon_{ljq} \sum_{n=1}^5 \gamma_{il}^{(n)}(\omega) + (i \leftrightarrow j)$ with all the 5 terms of $\gamma_{il}^{(n)}(\omega)$ listed in the Table. The terms $\gamma_{il}^{(n)}(\omega)$ consist of integrals over the Brillouin zone. In the integration, $\mathbf{A}_{ab,\mathbf{k}} = i \langle u_{a,\mathbf{k}} | \partial_{\mathbf{k}} u_{b,\mathbf{k}} \rangle$ is the non-Abelian Berry connection, $\hat{\partial}_{\mathbf{k}}$ denotes the generalized derivative operator, and $g_{ac,\mathbf{k}}^{(\nu)}$ with $\nu = 1, 2, 3$, $g_{acc_1,\mathbf{k}}^{(\nu')}$ with $\nu' = 4, 5$ are the frequency dependent form factors. The indices $i, l = x, y, z$ are the indices of spatial directions. All the integrands of $\gamma_{il}^{(n)}(\omega)$ respect the gauge invariance, so they are referred as the frequency dependent quantum geometric quantities. More details about the generalized derivative operator and the frequency dependent form factors can be found in the Supplemental Material [53].

Contributing terms	Frequency dependent quantum geometric quantities
$\gamma_{il}^{(1)}(\omega)$	$\int_{\mathbf{k}} \sum_a \partial_{k_i} f_{a,\mathbf{k}} \sum_{c \neq a} (i \mathbf{A}_{ac,\mathbf{k}} \times \mathbf{A}_{ca,\mathbf{k}})_l g_{ac,\mathbf{k}}^{(1)}(\omega)$
$\gamma_{il}^{(2)}(\omega)$	$\int_{\mathbf{k}} \sum_{a,c \neq a} f_{a,\mathbf{k}} i \left[A_{ac,\mathbf{k}}^i \left(\hat{\partial}_{\mathbf{k}} \times \mathbf{A}_{ca,\mathbf{k}} \right)_l - \left(\hat{\partial}_{\mathbf{k}} \times \mathbf{A}_{ac,\mathbf{k}} \right)_l A_{ca,\mathbf{k}}^i + \partial_{k_i} (\mathbf{A}_{ac,\mathbf{k}} \times \mathbf{A}_{ca,\mathbf{k}})_l \right] g_{ac,\mathbf{k}}^{(2)}(\omega)$
$\gamma_{il}^{(3)}(\omega)$	$\int_{\mathbf{k}} \sum_{a,c \neq a} f_{a,\mathbf{k}} [(i \mathbf{A}_{ac,\mathbf{k}} \times \mathbf{A}_{ca,\mathbf{k}})_l \Delta E_{ac,\mathbf{k}} \partial_{k_i} \Delta E_{ac,\mathbf{k}}] g_{ac,\mathbf{k}}^{(3)}(\omega)$
$\gamma_{il}^{(4)}(\omega)$	$\int_{\mathbf{k}} \sum_{a,c \neq a, c_1 \neq c, c_1 \neq a} f_{a,\mathbf{k}} [A_{cc_1,\mathbf{k}}^i (i \mathbf{A}_{ac,\mathbf{k}} \times \mathbf{A}_{c_1 a,\mathbf{k}})_l - A_{c_1 c,\mathbf{k}}^i (i \mathbf{A}_{ac_1,\mathbf{k}} \times \mathbf{A}_{ca,\mathbf{k}})_l] g_{acc_1,\mathbf{k}}^{(4)}(\omega)$
$\gamma_{il}^{(5)}(\omega)$	$\int_{\mathbf{k}} \sum_{a,c \neq a, c_1 \neq c, c_1 \neq a} f_{a,\mathbf{k}} [A_{ac,\mathbf{k}}^i (i \mathbf{A}_{cc_1,\mathbf{k}} \times \mathbf{A}_{c_1 a,\mathbf{k}})_l - (i \mathbf{A}_{ac_1,\mathbf{k}} \times \mathbf{A}_{c_1 c,\mathbf{k}})_l A_{ca,\mathbf{k}}^i] g_{acc_1,\mathbf{k}}^{(5)}(\omega)$

is constructed as

$$\sigma_{qij}^\perp(2\omega; \omega, \omega) = \frac{1}{3} [2\sigma_{qij}(2\omega; \omega, \omega) - \sigma_{ijq}(2\omega; \omega, \omega) - \sigma_{j iq}(2\omega; \omega, \omega)]. \quad (2)$$

It can be checked that $\sigma_{qij}^\perp(2\omega; \omega, \omega)$ meets the anti-symmetric requirement of the Hall conductivity while preserving the intrinsic permutation symmetry of i and j [53]. This way of constructing the nonlinear Hall conductivity is in the same spirit as the prescription introduced in Ref. [54], and one can further extend it to higher orders. Similar construction has also been done for the Hall component of the rectification conductivity (see the Supplemental Material [53]). Now, by combining Eq. 1 and Eq. 2, we are ready to present the complete expression for the second harmonic Hall conductivity.

Second harmonic Hall conductivity in insulators.— After the explicit calculation [53], we find that for a time reversal invariant system, the second harmonic Hall conductivity takes the form

$$\sigma_{qij}^\perp(2\omega; \omega, \omega) = \epsilon_{ljq} \gamma_{il}(\omega) + (i \leftrightarrow j), \quad (3)$$

with ϵ_{ljq} denoting the Levi-Civita symbol and $\gamma_{il}(\omega) = \int_{\mathbf{k}} \gamma_{il}(\omega, \mathbf{k}) = \sum_{n=1}^5 \gamma_{il}^{(n)}(\omega)$. The explicit expressions of $\gamma_{il}^{(n)}(\omega)$ are listed in Table I. It is clear that the integrand in $\gamma_{il}^{(n)}(\omega)$ is composed of a rank-2 pseudotensor multiplied by a frequency dependent form factor. The rank-2 pseudotensor takes the general form $v_i (\mathbf{v}_1 \times \mathbf{v}_2)_l$, with \mathbf{v} , \mathbf{v}_1 and \mathbf{v}_2 selected from the inter-band Berry connection $\mathbf{A}_{ab,\mathbf{k}}$ and the \mathbf{k} -space gradient $\partial_{\mathbf{k}}$. For the first term $\gamma_{il}^{(1)}(\omega)$, the gradient $\partial_{\mathbf{k}}$ acts on the distribution function $f_{a,\mathbf{k}}$, so $\gamma_{il}^{(1)}(\omega)$ purely accounts for the contribution from Fermi surfaces. In the low frequency limit $\omega \rightarrow 0$, $\gamma_{il}^{(1)}(\omega)$ reduces to the Berry curvature dipole [8].

The other terms $\gamma_{il}^{(n)}(\omega)$ with $n = 2, 3, 4, 5$, however, are more general combinations of $\partial_{\mathbf{k}}$, $\mathbf{A}_{ab,\mathbf{k}}$ and $f_{a,\mathbf{k}}$ that exclude $\partial_{\mathbf{k}} f_{a,\mathbf{k}}$, so the integrations in $\gamma_{il}^{(n)}(\omega)$ are over the occupied states. Here we have assumed that the system respects the time reversal symmetry, but one can generalize the combinations of $\partial_{\mathbf{k}}$, $\mathbf{A}_{ab,\mathbf{k}}$ and $f_{a,\mathbf{k}}$ in Table I to the case of time reversal symmetry breaking and higher order nonlinear Hall effect. Given a finite driving frequency, $\gamma_{il}^{(n)}(\omega)$ with $n = 2, 3, 4, 5$ are generally nonzero in an insulator. Importantly, near resonance $2\hbar\omega = \Delta$ (Δ denotes the band gap), $\gamma_{il}(\omega)$ in an insulator shows a substantial increase, as the inter-band processes get predominantly enhanced and contribute significantly to the nonlinear Hall effect. In an insulator, such nonvanishing nonlinear Hall effect near resonance actually manifests the breakdown of Kleinman symmetry [50–52].

The nonlinear Hall effect and the Kleinman symmetry.— In nonlinear optics, the Kleinman symmetry is known as the overall permutation symmetry of the susceptibility tensor in the frequency range far below resonances [51, 52]. For the SHG $P_q(2\omega) = \chi_{qij}(2\omega; \omega, \omega) \mathcal{E}_i(\omega) \mathcal{E}_j(\omega)$, the Kleinman symmetry states that the index q is commutative with i and j when $\hbar\omega \ll \Delta$. It is known that the conductivity and susceptibility of the SHG respect the intrinsic relation: $\sigma_{qij}(2\omega; \omega, \omega) = -i2\omega\epsilon_0\chi_{qij}(2\omega; \omega, \omega)$ with ϵ_0 being the vacuum permittivity, so the Kleinman symmetry precludes the nonlinear Hall effect in insulators when the driving frequency is far off resonance. However, the Kleinman symmetry is only an approximation valid in the far off resonant regime where the frequency dispersion of the media is negligible [51, 52]. As the driving frequency approaches resonance, inter-band processes get involved, resulting in significant frequency dispersion in the susceptibility. As a result, the Klein-

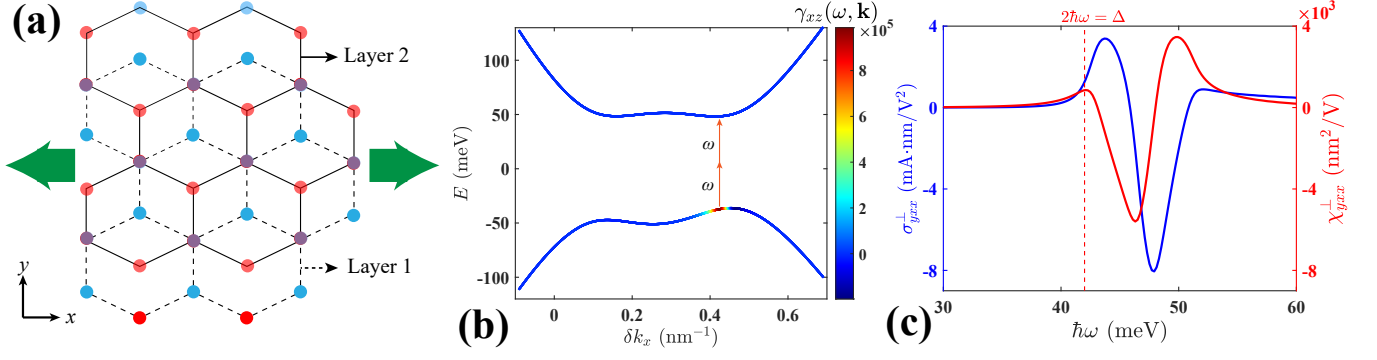


FIG. 2: The nonlinear Hall effect in an insulating strained Bernal bilayer graphene of C_{1v} symmetry. (a) The lattice structure of Bernal bilayer graphene with uniaxial strain applied along the zigzag direction (x -direction). (b) The band dispersions near the K valley ($\delta k_x = k_x - K_x$). A gap of $\Delta = 84$ meV is introduced by a z -directional electric field. The color variations denote $\gamma_{xz}(\omega, \mathbf{k})$, with $\hbar\omega = 42$ meV being the resonant frequency. Here $\gamma_{xz}(\omega, \mathbf{k})$ is in unit of $\text{mA}\cdot\text{nm}^3/\text{V}^2$. The strain amplitude is $\epsilon = 0.03$. (c) The second harmonic Hall conductivity $\sigma_{yxx}^\perp(2\omega; \omega, \omega)$ and susceptibility $\chi_{yxx}^\perp(2\omega; \omega, \omega)$ as functions of the driving frequency. The susceptibility $\chi_{yxx}^\perp(2\omega; \omega, \omega)$ reaches a local maxima at the resonant frequency, while the local maxima of $\sigma_{yxx}^\perp(2\omega; \omega, \omega)$ is achieved at a higher frequency. The relative shift of the peaks between $\sigma_{yxx}^\perp(2\omega; \omega, \omega)$ and $\chi_{yxx}^\perp(2\omega; \omega, \omega)$ stems from the frequency dependence in the definition: $\sigma_{yxx}^\perp(2\omega; \omega, \omega) = -i2\omega\epsilon_0\chi_{yxx}^\perp(2\omega; \omega, \omega)$. Due to the Mexican hat shape of the bands in (b), both $\sigma_{yxx}^\perp(2\omega; \omega, \omega)$ and $\chi_{yxx}^\perp(2\omega; \omega, \omega)$ show 3 local optimal values.

man symmetry breaks down and the nonlinear Hall effect arises near resonance.

Since the frequency dependence of susceptibility near resonance is inevitable for any insulator, insulators that respect the specific crystalline symmetry all have the nonlinear Hall effect. Among the 20 piezoelectric point groups that allow both the SHG and rectification [51, 52, 55], by applying Eq. 2, we find that the nonlinear Hall effect can exist in 16 point groups: C_n , C_{nv} , $D_{n'}$, D_{2d} and S_4 , with $n = 1, 2, 3, 4, 6$ and $n' = 2, 3, 4, 6$ [53]. The specific forms of the nonlinear Hall response tensor are presented in the Supplemental Materials [53]. The 16 point groups provide the guidance for seeking the nonlinear Hall effect in real insulators.

Application to the biased Bernal bilayer graphene under uniaxial strain.— To demonstrate the nonlinear Hall effect we propose in insulators, we calculate the second harmonic Hall conductivity in a biased Bernal bilayer graphene under uniaxial strain. The Bernal bilayer graphene originally respects the D_{3d} point group symmetry. After applying a z -directional electric field, the symmetry is reduced from D_{3d} to C_{3v} . The z -directional electric field introduces a gate tunable band gap [56–59]. Since the z -directional electric field breaks the inversion symmetry, the biased Bernal bilayer graphene can exhibit the SHG [60, 61]. Importantly, if a uniaxial strain is applied along the zigzag direction of the biased Bernal bilayer graphene (Fig. 2 (a)), its C_{3v} symmetry is further reduced to the C_{1v} that allows a nonzero nonlinear Hall effect. Recently, the nonlinear Hall effect has been observed in the metallic regime of a biased bilayer graphene under strain [34, 62]. It will be interesting to check the nonlinear Hall effect when the chemical potential is gate

tuned to lie inside the gap.

Our calculation results are shown in Fig. 2 (b) and (c), where the bias is set to induce a band gap $\Delta = 84$ meV, the chemical potential lies inside the gap, and the uniaxial strain $\epsilon = 0.03$ is applied along the zigzag direction. Fig. 2 (b) shows the band dispersions near K , where the color variations in the bands denote the \mathbf{k} -space distribution of $\gamma_{xz}(\omega, \mathbf{k})$. Here $\gamma_{xz}(\omega, \mathbf{k})$ is the integrand of $\gamma_{xz}(\omega)$. The nonzero values of $\gamma_{xz}(\omega, \mathbf{k})$ are mainly concentrated around the gap opening region (Fig. 2 (b)) [53], which indicates that the resulting nonlinear Hall effect is gate tunable. In Fig. 2 (c), it is clear to see that both $\sigma_{yxx}^\perp(2\omega; \omega, \omega)$ and $\chi_{yxx}^\perp(2\omega; \omega, \omega)$ vanish in the far off resonant regime. In the frequency range slightly below resonance, the susceptibility $\chi_{yxx}^\perp(2\omega; \omega, \omega)$ is significantly nonzero, and it reaches a local maxima at resonance $2\hbar\omega = \Delta$. The significantly nonzero $\chi_{yxx}^\perp(2\omega; \omega, \omega)$ with $\hbar\omega \in [36, 42]$ meV is purely reactive and involves no energy dissipation. In the frequency range $2\hbar\omega > \Delta$, inter-band transitions occur and give rise to the nonzero $\sigma_{yxx}^\perp(2\omega; \omega, \omega)$. It is worth noting that the Mexican hat shape of the band dispersions in Fig. 2 (b) provides 3 characteristic resonant frequencies [53], so $\sigma_{yxx}^\perp(2\omega; \omega, \omega)$ and $\chi_{yxx}^\perp(2\omega; \omega, \omega)$ in Fig. 2 (c) show 3 local optimal values. More analysis about the frequency dispersions of $\sigma_{yxx}^\perp(2\omega; \omega, \omega)$ and $\chi_{yxx}^\perp(2\omega; \omega, \omega)$ can be found in the Supplemental Materials [53]. Notably, the local maxima of $\chi_{yxx}^\perp(2\omega; \omega, \omega)$ at $\hbar\omega = 42$ meV reaches $800 \text{ nm}^2/\text{V}$, which is 2 orders larger than the SHG observed in the two dimensional transition metal dichalcogenides [63, 64]. This indicates that the Hall component of the SHG in the biased bilayer graphene under uniaxial strain is, in principle, measur-

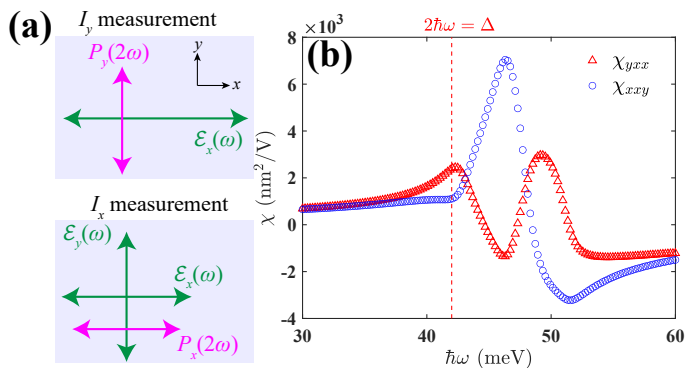


FIG. 3: Detection of the nonlinear Hall effect. (a) The schematic plot of the SHI measurement. The upper and lower panels correspond to the SHI measured in the y and x directions respectively. (b) The second harmonic susceptibility as a function of ω . In the far off-resonant regime, χ_{yxx} and χ_{xxy} are approximately the same value. As the driving frequency approaches resonance ($2\hbar\omega \rightarrow \Delta$), χ_{yxx} and χ_{xxy} start to differ significantly, which manifests the nonlinear Hall effect.

able in the Terahertz range.

To verify the nonlinear Hall effect in a material, one crucial step is to identify the anti-symmetric property of the nonlinear electric conductivity (or susceptibility). For the biased Bernal bilayer graphene under uniaxial strain in Fig. 2 (a), its C_{1v} symmetry dictates that the SHG takes the form [53]

$$P_x(2\omega) = \epsilon_0 \chi_{xxy}(2\omega; \omega, \omega) 2\mathcal{E}_x(\omega) \mathcal{E}_y(\omega), \quad (4)$$

$$P_y(2\omega) = \epsilon_0 \chi_{yxx}(2\omega; \omega, \omega) \mathcal{E}_x^2(\omega) + \epsilon_0 \chi_{yyy}(2\omega; \omega, \omega) \mathcal{E}_y^2(\omega). \quad (5)$$

The nonvanishing Hall component of the SHG arises from the fact that $\chi_{xxy}(2\omega; \omega, \omega) \neq \chi_{yxx}(2\omega; \omega, \omega)$ as $2\hbar\omega \rightarrow \Delta$. In practice, one can first identify the zigzag and armchair directions through the polarization resolved second harmonic microscopy [65–67]. After that, one can measure the second harmonic intensity (SHI) in the two orthogonal directions [53, 64]: 1) $P_y(2\omega) = \epsilon_0 \chi_{yxx}(2\omega; \omega, \omega) \mathcal{E}^2(\omega)$ induced by $\mathcal{E}(\omega) = [1, 0] \mathcal{E}(\omega)$, and 2) $P_x(2\omega) = \epsilon_0 \chi_{xxy}(2\omega; \omega, \omega) \mathcal{E}^2(\omega)$ induced by $\mathcal{E}(\omega) = \frac{1}{\sqrt{2}} [1, 1] \mathcal{E}(\omega)$, as schematically shown in Fig. 3 (a). The SHIs in the two directions are $I_x \propto P_x^2$, $I_y \propto P_y^2$, so the difference between I_x and I_y provides direct evidence of the nonlinear Hall effect. In Fig. 3 (b), the second harmonic susceptibility χ_{yxx} and χ_{xxy} are plotted as functions of ω . Consistent with our analysis, as $2\hbar\omega \rightarrow \Delta$, the deviation between χ_{yxx} and χ_{xxy} increases substantially, indicating the emergence of the nonlinear Hall effect. It is noteworthy that measuring the Terahertz conductivities of second order can also directly identify the nonlinear Hall effect [30, 68].

Discussions.— In this work, we pointed out that insulators can generally exhibit the nonlinear Hall effect

as long as their crystalline symmetry allows. We found that a series of frequency dependent quantum geometric quantities in the occupied bands play a pivotal role in generating the nonlinear Hall effect in insulators. In particular, we performed calculations on the gapped Bernal bilayer graphene with C_{1v} symmetry and demonstrated that the nonlinear Hall effect is pronounced at the driving frequency near resonance. Apart from the gapped Bernal bilayer graphene under uniaxial strain, quite a few two dimensional insulating materials fall into the category where the symmetry allows the nonlinear Hall effect. Candidates with remarkable nonlinear Hall effect in the insulating regime could be extended to the Moiré heterostructure of bilayer graphene [69, 70], atomically thin MoS₂ under uniaxial strain [71, 72], bilayer T_d-WTe₂ [73, 74], and in-plane ferroelectric monolayer SnTe [75, 76].

It is worth noting that the nonlinear Hall effect arising from the inter-band processes in insulators does not rely on the time reversal symmetry. In an insulator with multiple bands, frequency dispersions originate from the mismatch between the driving frequency and the multiple band gaps, so regardless of whether the insulator respects time reversal symmetry or not, the Kleinman symmetry can always break down near resonance, generating the nonzero nonlinear Hall conductivity. Here, we have mainly focused on the time reversal invariant insulators, but generalizing the formalism to the insulators with no time reversal symmetry [22, 77] is straightforward. Importantly, while the linear order intrinsic Hall effect in insulators requires time reversal symmetry breaking [78], the second order nonlinear Hall effect becomes the lowest order Hall effect permitted in a time reversal invariant insulator.

Finally, we would like to emphasize that insulators are completely reactive when the driving frequency is below resonance. For an insulator, the SHG below resonance corresponds to the forced vibration of the electric insulating ground state. Since the optical absorption is suppressed by the detuning gap, the energy dissipation involved in the SHG is tiny small. As a result, insulators with remarkable nonlinear Hall effect can be utilized to generate transverse second harmonics [79] with low energy dissipation.

Acknowledgements.— W.-Y.H. acknowledges the support from the National Natural Science Foundation of China (No. 12304200), the BHYJRC Program from the Ministry of Education of China (No. SPST-RC-10), and the start-up funding from ShanghaiTech University. K.T.L. acknowledges the support of the Ministry of Science and Technology, China, and Hong Kong Research Grant Council through Grants No. 2020YFA0309600, No. RFS2021-6S03, No. C6025-19G, No. C6053-23G, No. AoE/P-701/20, No. 16310520, No. 16307622 and No. 16309223.

- * hewy@shanghaitech.edu.cn
† phlaw@ust.hk
- [1] E. H. Hall, *Am. J. Math.* **2**, 287 (1879).
 - [2] E. Ramsden, *Hall Effect Sensors: Theory and Application* (Elsevier, New York, 2006).
 - [3] C.-Z. Chang, C.-X. Liu, and A. H. MacDonald, *Rev. Mod. Phys.* **95**, 011002 (2023).
 - [4] N. Nagaosa, J. Sinova, S. Onoda, A. H. MacDonald, and N. P. Ong, *Rev. Mod. Phys.* **82**, 1539 (2010).
 - [5] K. v. Klitzing, G. Dorda, and M. Pepper, *Phys. Rev. Lett.* **45**, 494 (1980).
 - [6] D. J. Thouless, M. Kohmoto, M. P. Nightingale, and M. den Nijs, *Phys. Rev. Lett.* **49**, 405 (1982).
 - [7] D. Xiao, M.-C. Chang, and Q. Niu, *Rev. Mod. Phys.* **82**, 1959 (2010).
 - [8] I. Sodemann and L. Fu, *Phys. Rev. Lett.* **115**, 216806 (2015).
 - [9] Y. Gao, S. A. Yang, and Q. Niu, *Phys. Rev. Lett.* **112**, 166601 (2014).
 - [10] C. Wang, Y. Gao, and D. Xiao, *Phys. Rev. Lett.* **127**, 277201 (2021).
 - [11] H. Liu, J. Zhao, Y.-X. Huang, W. Wu, X.-L. Sheng, C. Xiao, and S. A. Yang, *Phys. Rev. Lett.* **127**, 277202 (2021).
 - [12] D. Kaplan, T. Holder, and B. Yan, *Phys. Rev. Lett.* **132**, 026301 (2024).
 - [13] S. Nandy and I. Sodemann, *Phys. Rev. B* **100**, 195117 (2019).
 - [14] O. Matsyshyn and I. Sodemann, *Phys. Rev. Lett.* **123**, 246602 (2019).
 - [15] H. Liu, J. Zhao, Y.-X. Huang, X. Feng, C. Xiao, W. Wu, S. Lai, W. Gao, and S. A. Yang, *Phys. Rev. B* **105**, 045118 (2022).
 - [16] C.-P. Zhang, X.-J. Gao, Y.-M. Xie, H. C. Po, and K. T. Law, *Phys. Rev. B* **107**, 115142 (2023).
 - [17] Y. Fang, J. Cano, S. A. A. Ghorashi, *Phys. Rev. Lett.* **133**, 106701 (2024).
 - [18] R. Resta, *Phys. Rev. Research* **4**, 033002 (2022).
 - [19] Z. Z. Du, C. M. Wang, S. Li, H.-Z. Lu, and X. C. Xie, *Nat. Commun.* **10**, 3047 (2019).
 - [20] Z. Z. Du, C. M. Wang, H.-P. Sun, H.-Z. Lu, and X. C. Xie, *Nat. Commun.* **12**, 5038 (2021).
 - [21] M. S. Okyay, S. A. Sato, K. W. Kim, B. Yan, H. Jin, and N. Park, *Commun. Phys.* **5**, 303 (2022).
 - [22] D. Kaplan, T. Holder, and B. Yan, *Nat. Commun.* **14**, 3053 (2023).
 - [23] D. Mandal, S. Sarkar, K. Das, and A. Agarwal, arXiv: 2310.19092
 - [24] Z. Z. Du, H.-Z. Lu, and X. C. Xie, *Nat. Rev. Phys.* **3**, 744 (2021).
 - [25] C. Ortix, *Adv. Quantum Technol.* **4**, 2100056 (2021).
 - [26] A. Bandyopadhyay, N. B. Joseph, and A. Narayan, *Mater. Today Electro.* **8**, 100101 (2024).
 - [27] Q. Ma et al., *Nature* **565**, 337 (2019).
 - [28] K. Kang, T. Li, E. Sohn, J. Shan, and K. F. Mak, *Nat. Mater.* **18**, 324 (2019).
 - [29] S. Sinha et al., *Nat. Phys.* **18**, 765 (2022).
 - [30] A. Gao, Y.-F. Liu, J.-X. Qiu, B. Ghosh, T. V. Trevisan, Y. Onishi, C. Hu, T. Qian, H.-J. Tien, and S.-W. Chen et al., *Science* **381**, 181 (2023).
 - [31] N. Wang, D. Kaplan, Z. Zhang, T. Holder, N. Cao, A. Wang, X. Zhou, F. Zhou, Z. Jiang, and C. Zhang et al., *Nature* **621**, 487 (2023).
 - [32] P. He, S. S.-L. Zhang, D. Zhu, S. Shi, O. G. Heinonen, G. Vignale, and H. Yang, *Phys. Rev. Lett.* **123**, 016801 (2019).
 - [33] D. Kumar, C.-H. Hsu, R. Sharma, T.-R. Chang, P. Yu, J. Wang, G. Eda, G. Liang, and H. Yang, *Nat. Nanotech.* **16** 421, (2021).
 - [34] S.-C. Ho, C.-H. Chang, Y.-C. Hsieh, S.-T. Lo, B. Huang, T.-H.-Y. Vu, C. Ortix, and T.-M. Chen, *Nat. Electron.* **4**, 116 (2021).
 - [35] J. Duan, Y. Jian, Y. Gao, H. Peng, J. Zhong, Q. Feng, J. Mao, and Y. Yao, *Phys. Rev. Lett.* **129**, 186801 (2022).
 - [36] M. Huang et al., *Natl. Sci. Rev. nwc232* (2022).
 - [37] M. Huang, Z. Wu, X. Zhang, X. Feng, Z. Zhou, S. Wang, Y. Chen, C. Chen, K. Sun, Z. Y. Meng, and N. Wang, *Phys. Rev. Lett.* **131**, 066301 (2023).
 - [38] L. Min, H. Tan, Z. Xie, L. Miao, R. Zhang, S. H. Lee, V. Gopalan, C.-X. Liu, N. Alem, B. Yan, and Z. Mao, *Nat. Commun.* **14**, 364 (2023).
 - [39] X.-G. Ye, H. Liu, P.-F. Zhu, W.-Z. Xu, S. A. Yang, N. Shang, K. Liu, and Z.-M. Liao, *Phys. Rev. Lett.* **130**, 016301 (2023).
 - [40] B. Chen, Y. Gao, Z. Zheng, S. Chen, Z. Liu, L. Zhang, Q. Zhu, H. Li, L. Li, and C. Zeng, *Nat. Commun.* **15**, 5513 (2024).
 - [41] X. F. Liu, C.-P. Zhang, N. Wang, D. Zhao, X. Zhou, W. Gao, X. H. Chen, K. T. Law, and K. P. Loh, *Nat. Commun.* **15**, 245 (2024).
 - [42] S. Lai, H. Liu, Z. Zhang, J. Zhao, X. Feng, N. Wang, C. Tang, Y. Liu, K. S. Novoselov, S. A. Yang, and W. Gao, *Nat. Nanotechnol.* **16**, 869 (2021).
 - [43] S. Sankar et al., *Phys. Rev. X* **14**, 021046 (2024).
 - [44] I. Komissarov, T. Holder, and R. Queiroz, *Nat. Commun.* **15**4621 (2024).
 - [45] N. Verma and R. Queiroz, arXiv: 2403.07052
 - [46] D. J. Passos, G. B. Ventura, J. M. Viana Parente Lopes, J. M. B. Lopes dos Santos, and N. M. R. Peres, *Phys. Rev. B* **97**, 235446 (2018).
 - [47] J. E. Sipe and E. Ghahramani, *Phys. Rev. B* **48**, 11705 (1993).
 - [48] C. Aversa and J. E. Sipe, *Phys. Rev. B* **52**, 14646 (1995).
 - [49] G. B. Ventura, D. J. Passos, J. M. B. Lopes dos Santos, J. M. Viana Parente Lopes, and N. M. R. Peres, *Phys. Rev. B* **96**, 035431 (2017).
 - [50] D. A. Kleinman, *Phys. Rev. B* **128**, 1761 (1962).
 - [51] R. Boyd, *Nonlinear Optics* (Academic Press, 2020).
 - [52] P. N. Butcher and D. Cotter, *The Elements of Nonlinear Optics* (Cambridge University Press, 2003).
 - [53] See the Supplemental Materials for 1) more details about the density matrix formalism; 2) the decomposition of the nonlinear conductivity into the longitudinal and the transverse (Hall) components; 3) the explicit expressions for the Hall conductivity of the second harmonic generation; 4) the symmetry analysis of the nonlinear Hall response; 5) the calculations carried in the strained Bernal bilayer graphene of C_{1v} symmetry. The evolution of $\gamma_{xz}(\omega, \mathbf{k})$ as a function of the driving frequency ω is presented in a video attached in the Supplemental Materials.
 - [54] S. S. Tsirkin and I. Souza, *SciPost Phys. Core* **5**, 039 (2022).
 - [55] R. Newnham, *Properties of materials: anisotropy, symmetry and structure* (Oxford University Press Inc., New

- York, 2005).
- [56] K. F. Mak, C. H. Lui, J. Shan, and T. F. Heinz, *Phys. Rev. Lett.* **102**, 256405 (2009).
- [57] E. V. Castro, K. S. Novoselov, S. V. Morozov, N. M. R. Peres, J. M. B. Lopes dos Santos, J. Nilsson, F. Guinea, A. K. Geim, and A. H. Castro Neto, *Phys. Rev. Lett.* **99**, 216802 (2007).
- [58] Y. Zhang, T.-T. Tang, C. Girit, Z. Hao, M. C. Martin, A. Zettl, M. F. Crommie, Y. R. Shen, and F. Wang, *Nature* **459**, 820 (2009).
- [59] J. Velasco et al., *Nat. Nanotechnol.* **7**, 156 (2012).
- [60] S. J. Brun and T. G. Pedersen, *Phys. Rev. B* **91**, 205405 (2015).
- [61] R. McGouran and M. M. Dignam, *Phys. Rev. B* **96**, 045439 (2017).
- [62] R. Battilomo, N. Scopigno, and C. Ortix, *Phys. Rev. Lett.* **123**, 196403 (2019).
- [63] K. L. Seyler et al., *Nat. Nanotechnol.* **10**, 407 (2015).
- [64] S. Klimmer, O. Ghaebi, Z. Gan, A. George, A. Turchanin, G. Cerullo, and G. Soavi, *Nat. Photon.* **15**, 837 (2021).
- [65] N. Kumar, S. Najmaei, Q. Cui, F. Ceballos, P. M. Ajayan, J. Lou, and H. Zhao, *Phys. Rev. B* **87**, 161403 (R) (2013).
- [66] L. M. Malard, T. V. Alencar, A. P. M. Barboza, K. F. Mak, and A. M. de Paula, *Phys. Rev. B* **87**, 201401 (R) (2013).
- [67] Y. Li, Y. Rao, K. F. Mak, Y. You, S. Wang, C. R. Dean, and T. F. Heinz, *Nano Lett.* **13**, 3329 (2013).
- [68] S.-D. Chen, Q. Feng, W. Zhao, R. Qi, Z. Zhang, D. Abeyasinghe, C. Uzundal, J. Xie, T. Taniguchi, K. Watanabe, F. Wang, arXiv: 2409.17633
- [69] Z. Zheng, Q. Ma, Z. Bi, S. Barrera, M.-H. Liu et al., *Nature* **588**, 71 (2020).
- [70] R. Niu, Z. Li, X. Han, Z. Qu, D. Ding et al., *Nat. Commun.* **13**, 6241 (2022).
- [71] J. Lee, Z. Wang, H. Xie, K. F. Mak, and J. Shan, *Nat. Mater.* **16**, 887 (2017).
- [72] J. Son, K.-H. Kim, Y. H. Ahn, H.-W. Lee, and J. Lee, *Phys. Rev. Lett.* **123**, 036806 (2019).
- [73] H. Wang and X. Qian, *Npj Comput. Mater.* **5**, 119 (2019).
- [74] K. Kang, W. Zhao, Y. Zeng, K. Watanabe, T. Taniguchi, J. Shan, and K. F. Mak, *Nat. Nanotechnol.* **18**, 861 (2023).
- [75] K. Chang et al., *Science* **353**, 274 (2016).
- [76] J. Kim, K.-W. Kim, D. Shin, S.-H. Lee, J. Sinova, N. Park, and H. Jin, *Nat. Commun.* **10**, 3965 (2019).
- [77] P. He, H. Isobe, G. K. W. Koon, J. Y. Tan, J. Hu, J. Li, N. Nagaosa, and J. Shen, *Nat. Nanotechnol.* (2024), 10.1038/s41565-024-01730-1.
- [78] L. D. Landau, E. M. Lifshitz, and L. P. Pitaevskii, *Electrodynamics of Continuous Media*, 2nd ed. (Pergamon Press, Oxford, 1965), Vol. **8**.
- [79] M. W. Klein, C. Enkrich, M. Wegener, and S. Linden, *Science* **313**, 502 (2006).